Application of Three-dimensional IGN-2 Equations to Wave Diffraction Problems

Zhao, Binbin ; Zhang, Tianyu ; Duan, Wenyang ; Ertekin, R. Cengiz; Hayatdavoodi, Masoud

Published in:
Journal of Ocean Engineering and Marine Energy

DOI:
10.1007/s40722-019-00157-4

Publication date:
2019

Document Version
Peer reviewed version

Application of Three-dimensional IGN-2 Equations to Wave Diffraction Problems

Binbin Zhao[a], Tianyu Zhang[a], Wenyang Duan[a,*], R. Cengiz Ertekin[b,a], Masoud Hayatdavoodi[c,a]

[a] *College of Shipbuilding Engineering, Harbin Engineering University, 150001 Harbin, China*
[b] *Department of Ocean & Resources Engineering, University of Hawai'i, Honolulu, HI 96822, USA*
[c] *School of Science and Engineering, University of Dundee, Dundee DD1 4HN, UK*

Abstract

We use the Level II Irrotational Green-Naghdi (IGN-2) equations to study a number of wave diffraction problems. The IGN-2 equations can model strongly nonlinear waves. The three-dimensional solution of the IGN-2 equations is developed in this work and applied to some three-dimensional wave transformation and diffraction problems. Three test cases are considered. First one is on wave evolution in a closed basin. It is shown that the IGN-2 results agree well with the linear analytical results for small wave amplitudes. The following two cases involve wave diffraction problems caused by an uneven seabed. In both of these cases, excellent agreement is obtained between the IGN-2 model and the experimental measurements and numerical predictions of others. It is concluded that IGN-2 model can be used to accurately model diffraction and transformation of nonlinear waves in three dimensions.

Key words: Irrotational Green-Naghdi theory, IGN-2 equations, wave evolution, wave transformation, wave diffraction

1. Introduction

The Green-Naghdi (hereafter, GN) theory was first introduced about forty years ago (Green et al., 1974; Green and Naghdi, 1976). To derive the GN equations, a shape-function that approximates the vertical distribution of the velocity field along the water column is

*Corresponding author.

used. This is not the only way the GN equations can be derived, see, for example, the introduction sections of Kim et al. (2001) and Ertekin et al. (2014) for a discussion on the subject. In derivation of the GN equations, no other assumptions and approximations are introduced and no restriction is enforced on the rotationality of the flow field.

The GN theory is categorized into different levels, based on the approximation functions used to describe the distribution of the vertical velocity component along the water column. For example, Ertekin et al. (1986) utilized the Level I equations to simulate waves generated by ships in restricted waters. Demirbilek and Webster (1992) applied the Level II model to some two-dimensional wave propagation problems. The higher level GN wave equations have been developed and it is shown that they provide accurate results for strongly nonlinear and strongly dispersive waves (Zhao et al., 2014). The GN-1 equations were also used in three-dimensional problems, see Neill and Ertekin (1997), Ertekin and Sundararaghavan (2003), Hayatdavoodi et al. (2018), Neill et al. (2018). Zhao et al. (2015a) developed the three-dimensional solution method for the high-level GN equations. We note here that three-dimensionality refers to the physical problem, and not to the theory or the equations themselves, as the vertical structure of the flow field in the theory is known a priori.

Although irrotationality of the flow field is not a requirement in general in deriving the GN equation, it is possible to obtain the equations for an irrotational flow. Kim et al. (2001) derived the Irrotational Green-Naghdi (IGN) equations from Hamilton's principle. The IGN equations for finite water depth were numerically tested to show their self-convergence and accuracy in two dimensions (Kim et al., 2003, 2010). Polynomial expansions are used to prescribe the velocity field in vertical distribution. In the IGN models, only the odd terms of the polynomial are used. Zhao et al. (2015b) showed that the two-dimensional IGN equations are more efficient to solve than the GN equations where the rotationality of the flow is weak. However, the three-dimensional IGN equations have not been studied so far. Zhao et al. (2016) studied the IGN-2 equations and showed that IGN-2 equations are strongly nonlinear equations. The IGN-2 equations give errors of less than 2% in calculation of the phase velocity from shallow-water depths up to $kd = 4.87$, where k is the wave number and d is

the water depth. Higher level GN and IGN equations are strongly nonlinear and strongly dispersive wave equations.

The main motivation for this research is, therefore, to introduce the numerical model for three-dimensional IGN-2 equations and apply it to some water-wave diffraction problems. The intent of this paper is not to include very large waves and all the ranges of kd. In Section 2, the IGN equations are introduced. Section 3 presents the algorithm used in solving the IGN-2 equations. The solution of the linearised IGN-2 equations is given in Section 4. Some test cases simulated by the three-dimensional IGN-2 equations are presented in Section 5. These are followed by our conclusions in Section 6.

2. IGN equations

In this work, three-dimensional wave problems are considered. x and y are the horizontal coordinates, with x pointing to the right and y is into the paper, and z is the vertical coordinate, positive up. The origin of the right-handed coordinate system is located at the still-water level. The bottom boundary varies spatially, $z = -h(x, y)$. The free surface is specified by $z = \eta(x, y, t)$. The pressure on the free surface is taken as zero, i.e., $\hat{p}(x, y, t) = 0$, without loss in generality. The IGN equations used in this work are similar to those given by Ertekin et al. (2014) who presented the two-dimensional IGN equations.

In three dimensions, the velocity field (u, v, w) that satisfies the kinematic constraints are given by the stream function $\mathbf{\Psi}(x, y, z, t) = (\psi^u, \psi^v)$, where (u, v) are the horizontal components of velocity in the x and y direction, respectively, and w is the vertical component in the z direction. Therefore

$$(u, v) = \mathbf{\Psi}_{,z}, \tag{1a}$$

$$w = -\nabla \cdot \mathbf{\Psi}, \tag{1b}$$

Where ∇ is the gradient operator. Here, we make $\mathbf{\Psi}(x, y, z, t)$ equal to zero on the seabed,

i.e., $\boldsymbol{\Psi}(x, y, -h, t) = 0$. In the IGN theory, we assume that $\boldsymbol{\Psi}$ is given by

$$\boldsymbol{\Psi}(x, y, z, t) = \sum_{m=1}^{K} \boldsymbol{\Psi}_m(x, y, t) f_m(\gamma), \tag{2}$$

where $f_m(\gamma) = \gamma^{2m-1}$, $\gamma = (z + h)/(\eta + h)$ and $\boldsymbol{\Psi}_m$ are the unknown stream function coefficients which are calculated as part of the solution.

The IGN equations are given by two canonical equations for the free-surface elevation $\eta(x, y, t)$ and the surface velocity potential $\hat{\phi}(x, y, t)$:

$$\eta_{,t} + \sum_{m=1}^{K} f_m(1) \nabla \cdot \boldsymbol{\Psi}_m = 0, \tag{3a}$$

$$\hat{\phi}_{,t} = -\nabla \cdot \frac{\partial T}{\partial(\nabla \eta)} + \frac{\partial T}{\partial \eta} - g\eta\,, \tag{3b}$$

where T is the kinetic energy given by

$$\begin{aligned} T = \frac{1}{2} \sum_{m=1}^{K} \sum_{n=1}^{K} \{ & \theta A_{mn} (\nabla \cdot \boldsymbol{\Psi}_m)(\nabla \cdot \boldsymbol{\Psi}_n) \\ & + 2B_{mn} (\nabla \cdot \boldsymbol{\Psi}_m)(\boldsymbol{\Psi}_n \cdot \nabla h) - 2B^1_{mn} (\nabla \cdot \boldsymbol{\Psi}_m)(\boldsymbol{\Psi}_n \cdot \nabla \theta) \\ & + \frac{1}{\theta} C_{mn} \left[\boldsymbol{\Psi}_m \cdot \boldsymbol{\Psi}_n + (\nabla h \cdot \boldsymbol{\Psi}_m)(\nabla h \cdot \boldsymbol{\Psi}_n) \right] - \frac{2}{\theta} C^1_{mn} (\nabla h \cdot \boldsymbol{\Psi}_m)(\nabla \theta \cdot \boldsymbol{\Psi}_n) \\ & + \frac{1}{\theta} C^2_{mn} (\nabla \theta \cdot \boldsymbol{\Psi}_m)(\nabla \theta \cdot \boldsymbol{\Psi}_n) \} \,, \end{aligned} \tag{4}$$

where $\theta = \eta + h$ and

$$A_{mn} = \int_0^1 f_m(\gamma) f_n(\gamma) d\gamma \,, \tag{5a}$$

$$B_{mn} = \int_0^1 f_m(\gamma) f'_n(\gamma) d\gamma, \quad B^1_{mn} = \int_0^1 \gamma f_m(\gamma) f'_n(\gamma) d\gamma \,, \tag{5b}$$

$$C_{mn} = \int_0^1 f'_m(\gamma) f'_n(\gamma) d\gamma, \quad C^1_{mn} = \int_0^1 \gamma f'_m(\gamma) f'_n(\gamma) d\gamma \,, \tag{5c}$$

$$C^2_{mn} = \int_0^1 \gamma^2 f'_m(\gamma) f'_n(\gamma) d\gamma \,. \tag{5d}$$

Details of the derivation of the IGN equations can be found in Kim et al. (2001, 2003).

The IGN equations are completed by stating the relation between the surface velocity potential $\hat{\phi}(x, y, t)$ and the stream function coefficients $\boldsymbol{\Psi}_m$ $(m = 1, 2, \ldots, K)$:

$$f_m(1) \nabla \hat{\phi} = -\nabla \frac{\partial T}{\partial(\nabla \cdot \boldsymbol{\Psi}_m)} + \frac{\partial T}{\partial \boldsymbol{\Psi}_m} \quad (m = 1, 2, \ldots, K) \,. \tag{6}$$

Equations (3) and (6) constitute the three-dimensional IGN equations, and they are used to solve for η, $\hat{\phi}$ and $\mathbf{\Psi}_m$ $(m = 1, 2, \ldots, K)$. In addition, K stands for the level of IGN equations. For example, $K = 1, K = 2, K = 3$ represent IGN-1 equations, IGN-2 equations, IGN-3 equations, respectively. Here, we focus on the IGN-2 equations.

3. Solution Algorithm

For the IGN-2 equations, Eq. (6) in the x and y directions can be expressed by

$$\tilde{\mathbf{A}}^u \boldsymbol{\xi}^u_{,xx} + \tilde{\mathbf{B}}^u \boldsymbol{\xi}^u_{,x} + \tilde{\mathbf{C}}^u \boldsymbol{\xi}^u = \tilde{\mathbf{f}}^u \,, \tag{7a}$$

$$\tilde{\mathbf{A}}^v \boldsymbol{\xi}^v_{,yy} + \tilde{\mathbf{B}}^v \boldsymbol{\xi}^v_{,y} + \tilde{\mathbf{C}}^v \boldsymbol{\xi}^v = \tilde{\mathbf{f}}^v \,, \tag{7b}$$

where the superscript u and v are used to differentiate the x and y directions in Eq. (6), $\boldsymbol{\xi}^u = [\psi_1^u, \psi_2^u]^T$ and $\boldsymbol{\xi}^v = [\psi_1^v, \psi_2^v]^T$. The subscript after comma stands for differentiation with respect to the indicated variable. $\boldsymbol{\xi}^u_{,x}$ and $\boldsymbol{\xi}^u_{,xx}$, for example, indicate the first and second derivatives of $\boldsymbol{\xi}^u$, respectively.

In Eq. (7), $\tilde{\mathbf{A}}^u$, $\tilde{\mathbf{B}}^u$, $\tilde{\mathbf{C}}^u$, $\tilde{\mathbf{A}}^v$, $\tilde{\mathbf{B}}^v$ and $\tilde{\mathbf{C}}^v$ are 2×2 matrices. They are functions of h, η and their spatial derivatives. $\tilde{\mathbf{f}}^u$ and $\tilde{\mathbf{f}}^v$ are 2-dimensional vectors. $\tilde{\mathbf{f}}^u$ are functions of h, η, $\boldsymbol{\xi}^v$ and their spatial derivatives. $\tilde{\mathbf{f}}^v$ are functions of h, η, $\boldsymbol{\xi}^u$ and their spatial derivatives.

The finite central-difference method is used here for spatial derivatives. The (x, y) domain is uniformly discretized in the calculations by $(\Delta x, \Delta y)$ intervals. The discretized point on the grid is denoted by $x_i = i\Delta x$ for $i = 1, 2, \cdots, n_x$ and $y_j = j\Delta y$ for $j = 1, 2, \cdots, n_y$. Time is discretized with intervals of Δt such that $t_k = k\Delta t$ for $k = 1, 2, \cdots$.

For a given j, $\boldsymbol{\xi}^u(i, j)(i = 1, 2, \ldots, n_x)$ can be obtained by solving Eq. (7a). Similarly, for a given i, we can obtain $\boldsymbol{\xi}^v(i, j)(j = 1, 2, \ldots, n_y)$ from Eq. (7b). Further details of the numerical solution of Eq. (7a) can be found in Zhao et al. (2014).

We use the fourth-order Adams predictor-corrector scheme to march in time. They are

$$\eta^k = \eta^{k-1} + (55\eta_{,t}{}^{k-1} - 59\eta_{,t}{}^{k-2} + 37\eta_{,t}{}^{k-3} - 9\eta_{,t}{}^{k-4})\Delta t/24 \,, \tag{8a}$$

$$\eta^k = \eta^{k-1} + (9\eta_{,t}{}^{k} + 19\eta_{,t}{}^{k-1} - 5\eta_{,t}{}^{k-2} + \eta_{,t}{}^{k-3})\Delta t/24 \,, \tag{8b}$$

where k indicates the time step in $t_k = k\Delta t$ for $k = 1, 2, \cdots$. Similarly, $\hat{\phi}$ can also be predicted and corrected.

The wave maker is based on the solution of the linearised IGN-2 equations and this will be discussed in the next Section. For the cases studied here, two wave-absorbing regions are used: one near the wave-maker to prevent the reflected waves from interfering with the wave-maker, and the other one to absorb waves at the opposite end of the domain, see Zhao et al. (2014, 2015a) for more details.

4. Solution of the linearised IGN-2 equations

To obtain the solution of the linearised IGN-2 equations, we use the one-dimensional (horizontal component) IGN equations and set the water depth to a constant $h(x) = d$. First, we linearize Eq. (3b) to obtain

$$\hat{\phi}_{,t} = -g\eta(x,t)\,. \tag{9}$$

We assume that the change of the wave surface elevation can be described by a cosine function:

$$\eta = A\cos(k(x-ct))\,, \tag{10}$$

where k is the wave number and c the wave speed. Then, from Eq. (9)

$$\hat{\phi} = \frac{Ag}{ck}\sin(k(x-ct))\,. \tag{11}$$

We can also obtain the linearized form of Eq. (6). They are given as

$$-\hat{\phi}_{,x}(x,t) + \frac{\psi_1(x,t)}{d} + \frac{\psi_2(x,t)}{d} - \frac{1}{3}d{\psi_1}^{(2,0)}(x,t) - \frac{1}{5}d{\psi_2}^{(2,0)}(x,t) = 0\,, \tag{12a}$$

$$-\hat{\phi}_{,x}(x,t) + \frac{\psi_1(x,t)}{d} + \frac{9\psi_2(x,t)}{5d} - \frac{1}{5}d{\psi_1}^{(2,0)}(x,t) - \frac{1}{7}d{\psi_2}^{(2,0)}(x,t) = 0\,. \tag{12b}$$

We assume that the coefficient ψ_1 and ψ_2 change as

$$\psi_1 = Q_1\cos(k(x-ct))\,, \tag{13a}$$

$$\psi_2 = Q_2\cos(k(x-ct))\,. \tag{13b}$$

Substituting Eqs. (13) and (11) into Eq. (12) gives

$$-\frac{Ag}{c}+\frac{Q_1}{d}+\frac{1}{3}dk^2Q_1+\frac{Q_2}{d}+\frac{1}{5}dk^2Q_2=0\,, \tag{14a}$$

$$-\frac{Ag}{c}+\frac{Q_1}{d}+\frac{1}{5}dk^2Q_1+\frac{9Q_2}{5d}+\frac{1}{7}dk^2Q_2=0\,. \tag{14b}$$

Equations (14) can be written as

$$Q_1=-\frac{15Adg(-14+d^2k^2)}{2c(105+45d^2k^2+d^4k^4)}\,, \tag{15a}$$

$$Q_2=\frac{35Ad^3gk^2}{2c(105+45d^2k^2+d^4k^4)}\,. \tag{15b}$$

On the other hand, Eq. (3a) can be written as

$$\eta^{(0,1)}(x,t)+{\psi_1}^{(1,0)}(x,t)+{\psi_2}^{(1,0)}(x,t)=0\,. \tag{16}$$

Substituting Eqs. (15) and (13) into Eq. (16) gives

$$c^2=\frac{5(21dg+2d^3gk^2)}{105+45d^2k^2+d^4k^4}\,. \tag{17}$$

The nondimensional form of c^2 is

$$\bar{c}^2=\frac{5(21+2\bar{k}^2)}{105+45\bar{k}^2+\bar{k}^4}\,, \tag{18}$$

where the constant water depth d and gravitational acceleration g are used to obtain the nondimensional Eq. (18).

The Airy wave theory (or linear water wave theory) gives the linear dispersion relation (see for example Wiegel (1964))

$$\bar{c}^2_{Airy}=\tanh(\bar{k})/\bar{k}\,. \tag{19}$$

In Fig. 1, it is shown that the relation between c/c_{Airy} and kh is predicted by the linearised IGN-2 equations. We observe that the IGN-2 equations give errors of less than 2% in the phase velocity from shallow-water depths up to $kd=4.87$. We also note that the IGN-2 equations have no restriction on the wave amplitude. They can be used to simulate waves up to the breaking point.

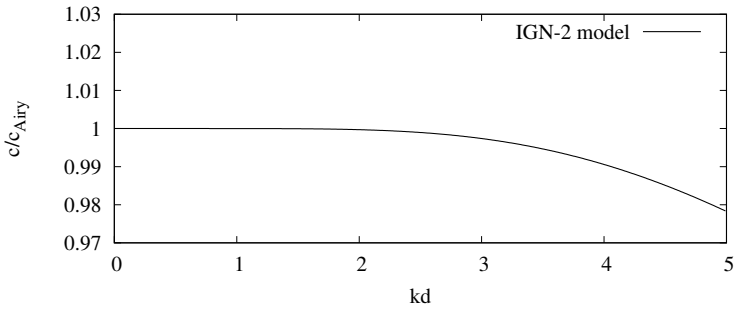

Figure 1: Linear dispersion relation of the IGN-2 model.

5. Test cases

In this section, we will present results of the IGN-2 equations in three dimensions for three different cases. The results are compared with some existing laboratory experiments, and with the available theoretical and numerical solutions of the problems.

5.1. Wave evolution in a closed basin

To study the accuracy of the three-dimensional IGN-2 equations and the numerical model used here, we first consider the problem of wave evolution in a closed basin with $L_x = L_y = 7.5m$, where L_x and L_y are the length and width of the basin, respectively.

The domain is extended between $-L_x/2 \leq x \leq L_x/2$ and $-L_y/2 \leq y \leq L_y/2$ with reflective vertical walls. The initial condition is a surface elevation of Gaussian shape $\eta_0(x, y)$ above an otherwise constant water depth $h_0 = 0.45m$. $\eta_0(x, y)$ is defined by

$$\eta_0(x, y) = H_0 \exp[-2(x^2 + y^2)]\,, \tag{20}$$

where $H_0 = 0.1h_0 = 0.045m$ in this case. Grid size of $\Delta x = \Delta y = 0.15m$ and time step size of $\Delta t = 0.05s$ are used. The IGN-2 results are compared with the linear analytical solution of this problem (Wei and Kirby, 1995). The comparison on wave elevation at two points is shown in Fig. 2. These two points are: point (a) at $x = 0m$ and $y = 0m$, i.e., the center of the computational domain, and point (b) at $x = -L_x/2$ and $y = -L_y/2$, i.e., the corner.

Due to the small initial wave amplitude, $H_0 = 0.1h_0$, the agreement between IGN-2 results and the linear solution of the problem is very good. The initial elevation is symmetric about

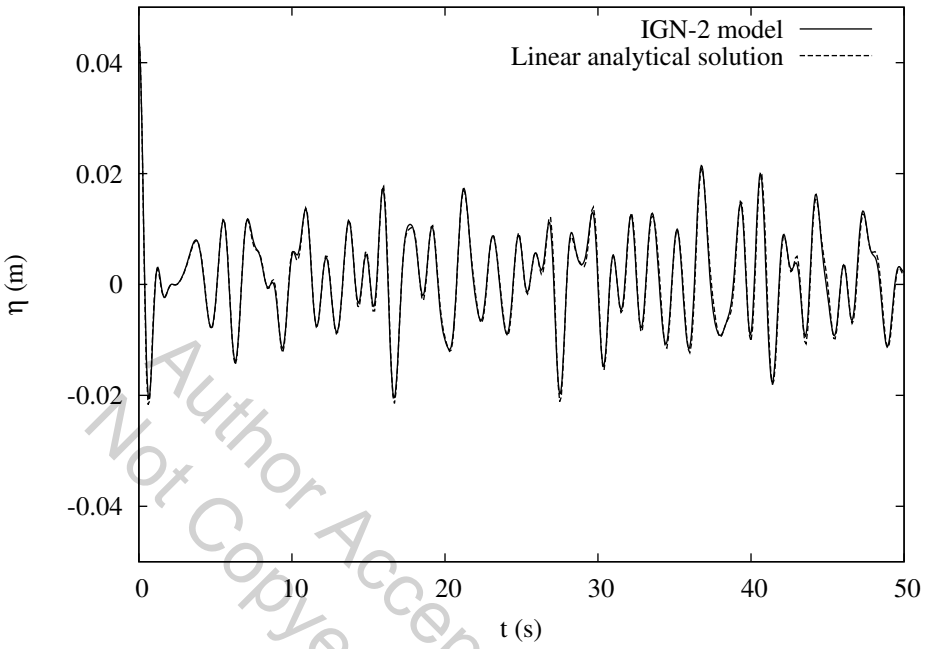

(a) $x = 0$m and $y = 0$m

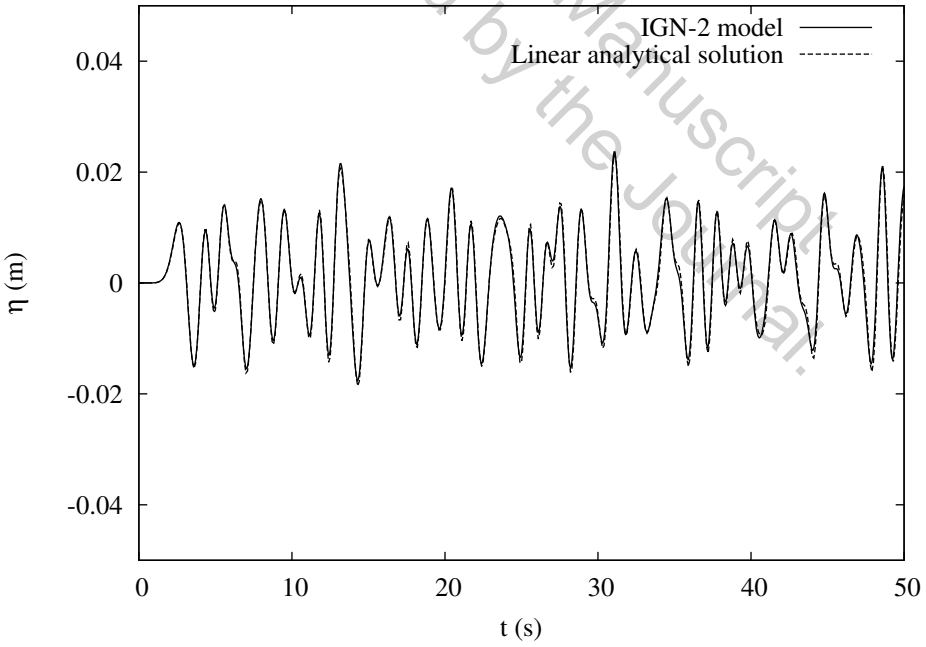

(b) $x = -L_x/2$ and $y = -L_y/2$

Figure 2: Time histories of wave elevation at two points ((a) center and (b) corner of the basin).

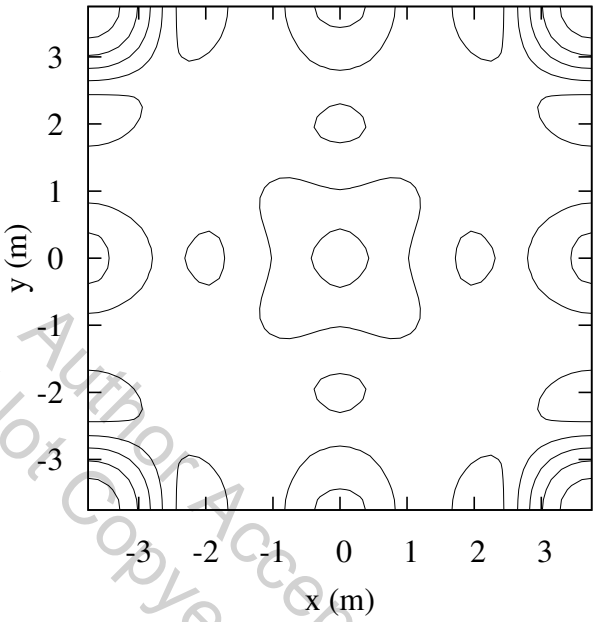

Figure 3: Surface contour of the IGN-2 model, illustrating rotational symmetry of evolving waves.

the center of the basin ($x = 0m$, $y = 0m$.) As a result, the surface elevation at anytime should be symmetric about the center. The contours of the free surface at $t = 50s$ are calculated by the IGN-2 equations; they are shown in Fig. 3. We observe that the contours of wave evolution is symmetric about the center of the basin.

We also checked the mass conservation. Since no water can escape the numerical basin, the water volume should remain constant in our calculations, and it is indeed determined to be constant. In addition, the computational time of this case is within 1 minutes on Inter(R) Core(TM) i7-7700 CPU @ 3.60GHz processor.

5.2. Wave transformation over a circular shoal (Chawla and Kirby, 1996)

Chawla and Kirby (1996) conducted a series of physical experiments for wave transformation over a circular shoal. Their experiments consist of test cases of regular waves and directional random waves, including breaking and nonbreaking waves. To study the com-

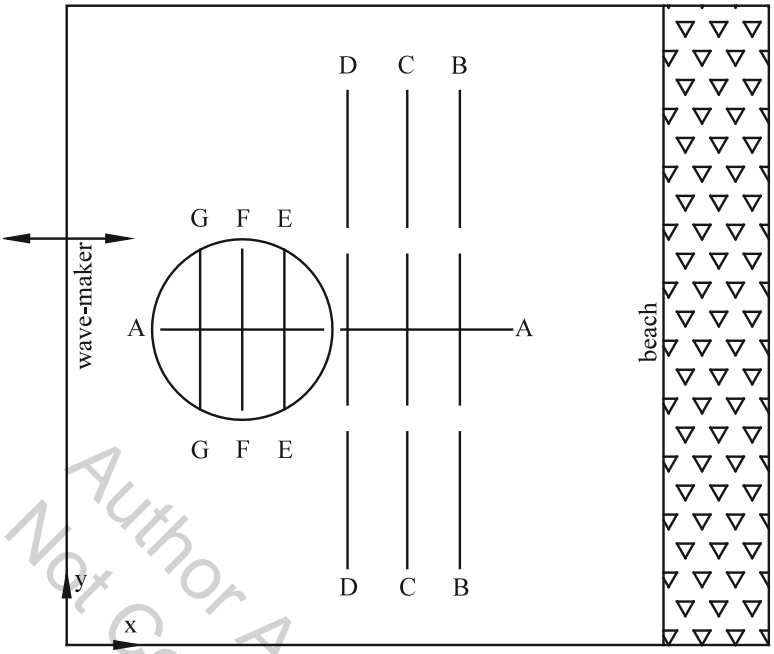

Figure 4: Experimental setup of wave transformation over a circular shoal of Chawla and Kirby (1996).

bined wave refraction/diffraction in two horizontal dimensions, we present comparisons with the nonbreaking monochromatic wave cases.

The dimensions of the physical wave tank used by Chawla and Kirby (1996) is $0 \leq x \leq 20m$ and $0 \leq y \leq 18.2m$; a circular shoal is placed on an otherwise flat bottom in the basin, as shown in Fig. 4. The center of the shoal is located at $x = 5m$ and $y = 8.98m$. The perimeter of the shoal is defined by

$$(x-5)^2 + (y-8.98)^2 = (2.57)^2. \tag{21}$$

The water depth on the submerged shoal is given by

$$h = h_0 + 8.73 - \sqrt{82.81 - (x-5)^2 - (y-8.98)^2}\,, \tag{22}$$

where $h_0 = 0.45m$ is the constant water depth of the basin.

In our numerical calculations, we extend the domain to $-2 \leq x \leq 33m$ to avoid reflections contaminate the interior results. We confine our attention to waves in the range of $0 \leq x \leq 20m$. Whereas $-2 \leq x \leq 2m$ region is used to absorb the reflected waves by the shoal back to the wave-maker, and $29 \leq x \leq 33m$ region is used to absorb the waves on the right end

of the domain. At $x = -2m$, monochromatic waves are generated, and they propagate in the positive x direction over the circular shoal. The wave height of the incoming waves is $H_0 = 1.18cm$, and the wave period is $T = 1.0s$. At the wave maker, $kh = 1.89$, which is within the limits of the IGN-2 equations.

On the top of the circular shoal, the water depth is $h = 8cm$. We choose a uniform grid spacing of $\Delta x = \Delta y = 0.1m$ in both the x and y directions. A time step of $\Delta t = 0.0333s$ is used. The comparison of the relative wave height (H/H_0) between the IGN-2 equations and the fully nonlinear Boussinesq equations of Chen et al. (2000), and the laboratory measurements of Chawla and Kirby (1996) at different locations in the tank is shown in Fig. 5.

From Fig. 5, a close agreement between the IGN-2 results and the experimental data of Chawla and Kirby (1996) is observed. In this case, the H/H_0 ratio reaches the value of $H/H_0 = 2.7$, as seen in Fig. 5(a). The results for H/H_0 from the Boussinesq equations (Chen et al., 2000) go to zero at the end of tank, while IGN-2 results do not approach zero. Note that the numerical wave tank in Chen et al. (2000) is $20m$ long and waves are absorbed before $x = 20m$. In our calculations, however, the numerical tank is much longer and the waves are not absorbed at $x = 20m$. The close agreement between the IGN-2 and the Boussinesq equations (Chen et al., 2000) observed along the transects at $x = 3.8m$, $x = 5.0m$, $x = 6.2m$, $x = 8.0m$, $x = 9.7m$ and $x = 11.2m$ (see Figs. 5(b)-5(g)) implies that the combined refraction/diffraction effects are captured successfully by these equations. The shoal center is located at the $y = 8.98m$ (the width of the tank is $18.2m$), which is slightly closer to one of the side walls ($y = 0m$). Therefore, the distribution of wave height in the y direction is not symmetric; this can be observed in Figs. 5(b)-5(g). In addition, the computational time is less than 10 minutes.

5.3. Wave transformation over a semi-circular shoal (Whalin, 1971)

Whalin (1971) conducted a series of laboratory experiments on wave convergence over a bottom topography. The size of the tank is $0m \leq x \leq 25.603m$ and $0m \leq y \leq 6.096m$. The

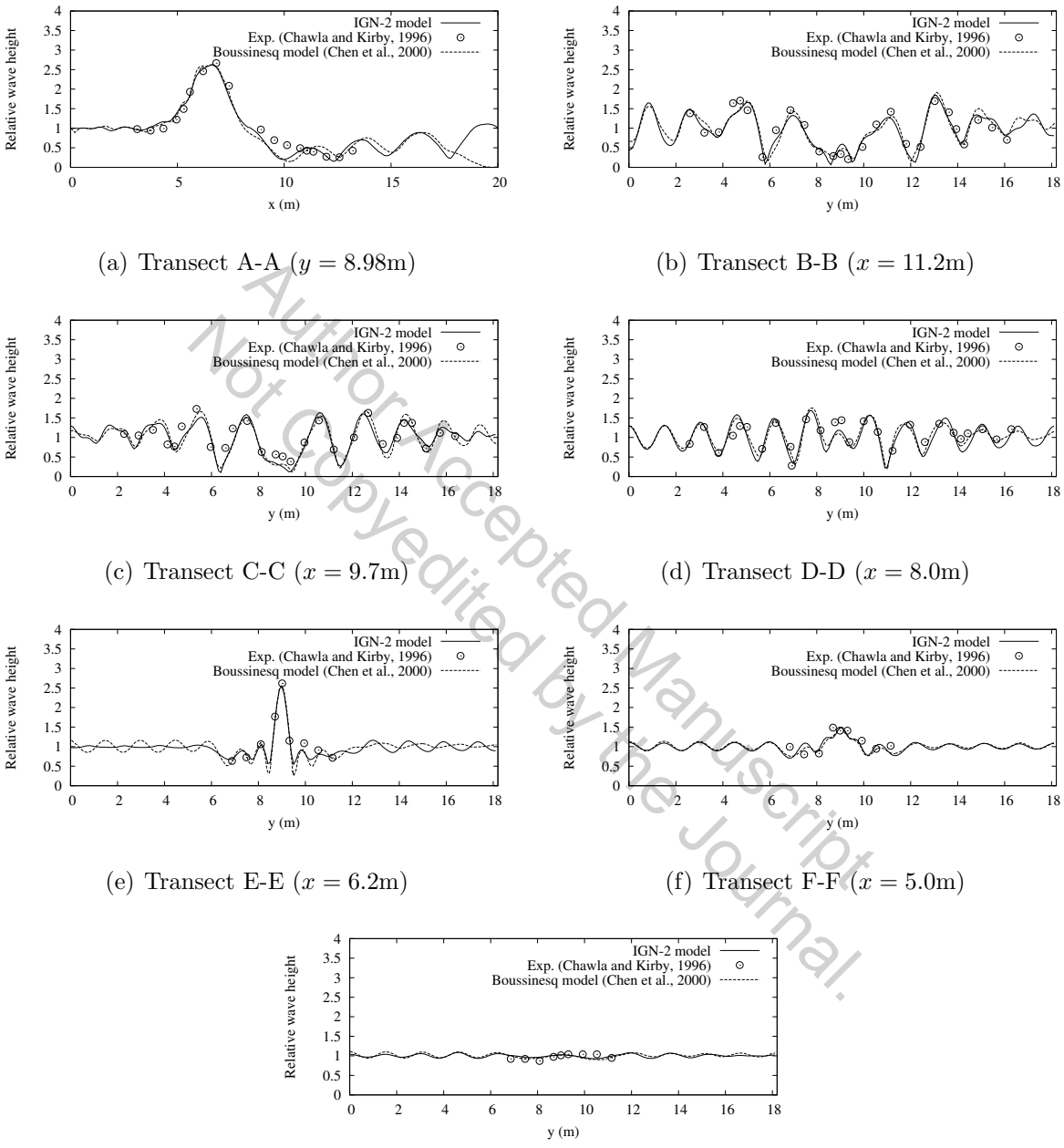

(a) Transect A-A ($y = 8.98$m)

(b) Transect B-B ($x = 11.2$m)

(c) Transect C-C ($x = 9.7$m)

(d) Transect D-D ($x = 8.0$m)

(e) Transect E-E ($x = 6.2$m)

(f) Transect F-F ($x = 5.0$m)

(g) Transect G-G ($x = 3.8$m)

Figure 5: Comparison of relative wave height calculated by the IGN-2 model with laboratory measurements of Chawla and Kirby (1996) and numerical results of Chen et al. (2000).

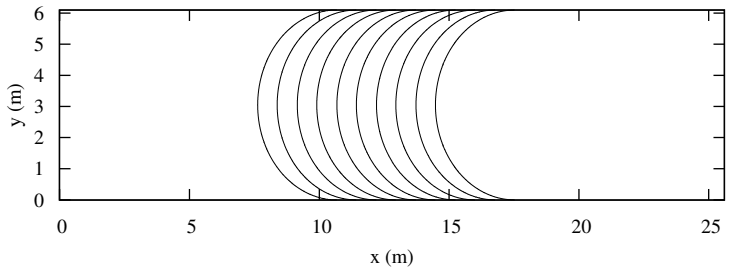

Figure 6: Setup of the wave tank of Whalin (1971).

bathymetry is shown in Fig. 6. The equations approximating the bathymetry are given as follows (Whalin, 1971):

$$h(x,y) = \begin{cases} 0.4572 & (x \le 10.67 - G) \\ 0.4572 + \frac{1}{25}\left(10.67 - G - x\right) & (10.67 - G \le x \le 18.28 - G) \\ 0.1524 & (x \ge 18.28 - G) \end{cases} \tag{23a}$$

$$G(y) = \sqrt{y(6.096 - y)} \quad (0 \le y \le 6.096)\,, \tag{23b}$$

where x and y are measured in meter. A semi-circular shoal is used to connect the deep part of the basin with the shallow part.

Whalin (1971) conducted three sets of experiments by generating waves in the deeper part of the model with periods of $1s$, $2s$ and $3s$. This case is considered by many as a benchmark experiment for their numerical models. For example, Rygg (1988), Kennedy and Fenton (1996), Li and Fleming (1997), Eskilsson and Sherwin (2006), Engsig-Karup et al. (2008), Bingham et al. (2009), Young et al. (2009), and others, compared their numerical results with these experimental data.

Here, we use the results of Rygg (1988), Li and Fleming (1997) and Bingham et al. (2009) to perform a comparative study. Rygg (1988) tested the classical Boussinesq equations against the experimental data for nonlinear waves of periods $2s$ and $3s$. Li and Fleming (1997) developed a three-dimensional multigrid model for fully nonlinear water waves. Bingham et al. (2009) tested the highly accurate Boussinesq-type model against some of the experimental data. The incoming wave parameters studied here are shown in Table 1.

Case	T(s)	A(cm)	Boussinesq model (Rygg, 1988)	Fully nonlinear multigrid model (Li and Fleming, 1997)	Highly accurate Boussinesq models (Bingham et al., 2009)
1	1	0.97	—	Fig. 10	—
2	1	1.95	—	Fig. 11	Fig. 6
3	2	0.75	Fig. 5	Fig. 12	Fig. 7
4	2	1.06	Fig. 6	Fig. 13	—
5	2	1.49	Fig. 7	Fig. 14	—
6	3	0.68	Fig. 8	Fig. 15	Fig. 8
7	3	0.98	Fig. 9	Fig. 16	—
8	3	1.46	Fig. 10	Fig. 17	—

Table 1: Wave conditions of Whalin (1971) and numerical models of others

Due to the symmetry along $y = 3.048m$, only half of the y region is considered in our calculations. In all the numerical calculations, the spatial step is $\Delta x = \Delta y = 0.1016m$ and the time step is $\Delta t = 0.025s$. An FFT analysis of the time series was made for each grid at the central line of the wave tank ($y = 3.048m$). The numerical results are compared with the experimental data and presented in Figs. 7-14.

In Case 1 ($T = 1.0s$ and $a = 0.0097m$), shown in Table 1, the IGN-2 results are close to the experimental data, see Fig. 7. As waves refract over the topography and focus along the centerline of the tank, a significant amount of energy is transferred into the higher-harmonic components. We also observe that the agreement of the IGN-2 results with the experimental data is better than the results of Li and Fleming (1997).

For Case 2 ($T = 1.0s$ and $a = 0.0195m$), the IGN-2 results are also in good agreement with the experimental data, see Fig. 8. The highly accurate Boussinesq results (Bingham et al., 2009) agree very well with the IGN-2 results. The small differences between the IGN-2 results and the highly accurate Boussinesq results are mainly caused by the reflections from

198 the right side of the Boussinesq calculations. In the IGN-2 calculations, the length of the tank
199 is set long enough to avoid reflections. We also observe that both the IGN-2 results and the
200 highly accurate Boussinesq results are in better agreement with the laboratory measurements
201 than the fully nonlinear multigrid model results of Li and Fleming (1997).

202 For the case of $T = 2s$, the IGN-2 results are shown in Figs. 9-11. We observe that
203 the IGN-2 results agree well with the experimental data. The solutions of the Boussinesq
204 equations (Rygg, 1988) and the fully nonlinear multigrid model (Li and Fleming, 1997) are
205 used for comparisons. For Cases 3-5, the fully nonlinear multigrid results (Li and Fleming,
206 1997) do not agree well with the experimental data. The results from Boussinesq equations
207 (Rygg, 1988) are better than the fully nonlinear multigrid model results (Li and Fleming,
208 1997). The results of the higher-harmonic amplitudes predicted by the Boussinesq equations
209 (Rygg, 1988) are lower than those of the IGN-2.

210 For Case 3, we compare the IGN-2 results with the highly accurate Boussinesq results
211 (Bingham et al., 2009). Very good agreement is observed, and this indicates that the IGN-2
212 results here are more accurate than the Boussinesq equations of Rygg (1988) in this case.
213 We also observe that when the wave amplitude increases, the second harmonic amplitudes
214 increase significantly, see Figs. 9(b), 10(b), 11(b). Similarly, the third harmonic amplitudes
215 increase. Keeping more harmonic components in the analysis seems to be more reasonable,
216 and in our calculations we considered up to the fifth harmonics.

217 For the case of $T = 3s$, the IGN-2 results are shown in Figs. 12-14, and they agree
218 well with the experimental data. It is also observed that there are some differences between
219 the numerical results of all models and the experimental data. In the paper by Bingham
220 et al. (2009), they reproduced Case 6 and they also observed that there are some differences
221 between their highly accurate Boussinesq results and the experimental data. For the cases of
222 $T = 3s$, there is significant reflection from the right side during the experiments. The reflected
223 energy propagates back to the wave maker and possibly interfere with the wave generation in
224 the physical experiments. In our numerical calculation, we use two wave-absorbing regions
225 as mentioned at the end of Section 3. This may explain the larger differences seen for this

case.

For Case 6, the results of highly accurate Boussinesq (Bingham et al., 2009) and the present IGN-2 results are in good agreement. For Cases 6-8, the results from Boussinesq equations of Rygg (1988) and the present IGN-2 results are in good agreement. The fully nonlinear multigrid model results of Li and Fleming (1997) do not show good accuracy compared with the other numerical results.In addition, the computational time of each case is less than 6 minutes.

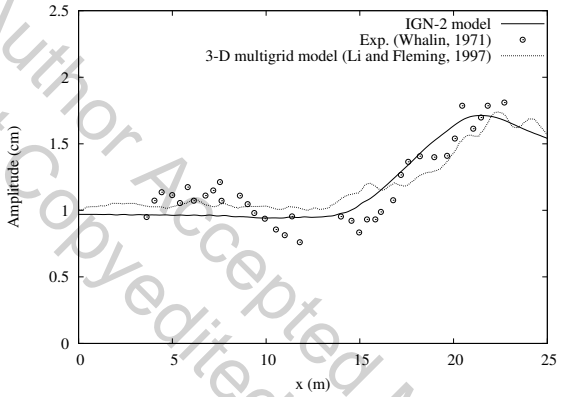

(a) 1st harmonic

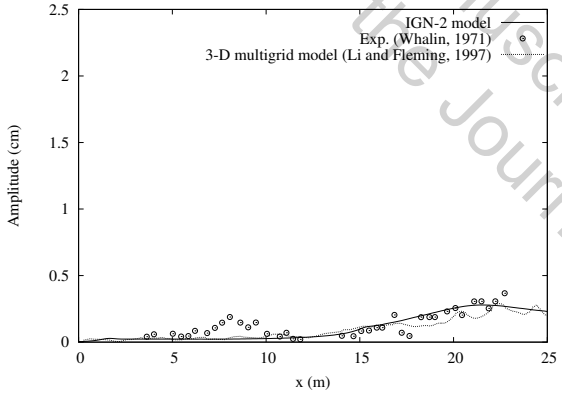

(b) 2nd harmonic

Figure 7: Wave amplitudes along the centerline of the wave tank for Case 1.

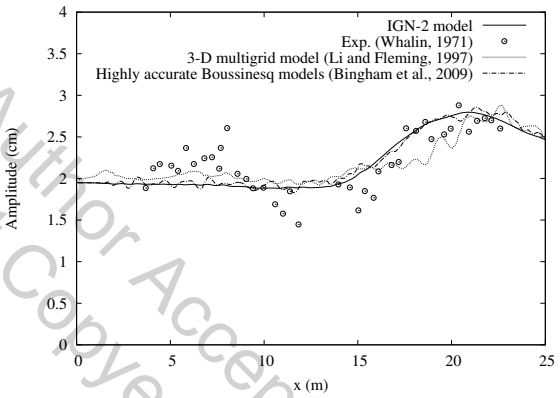

(a) 1st harmonic

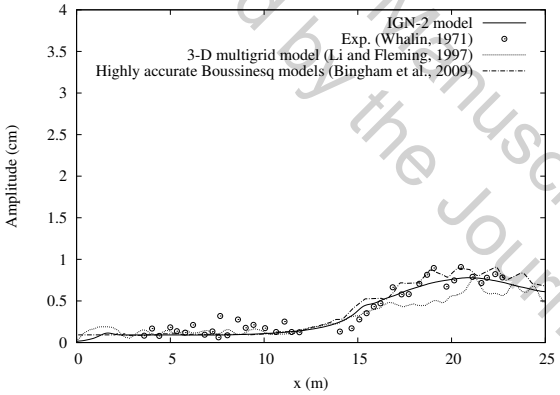

(b) 2nd harmonic

Figure 8: Wave amplitudes along the centerline of the wave tank for Case 2.

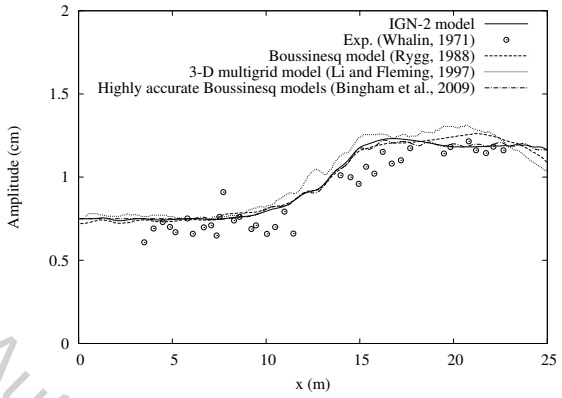

(a) 1st harmonic

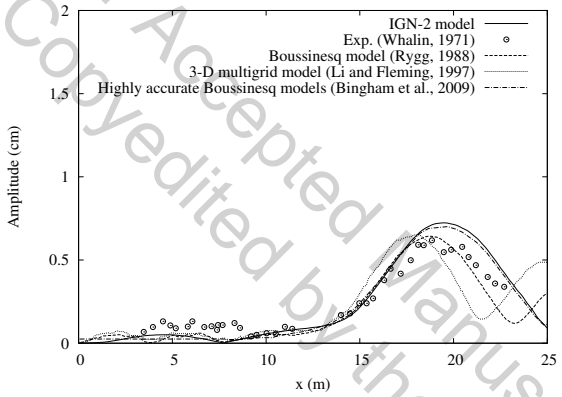

(b) 2nd harmonic

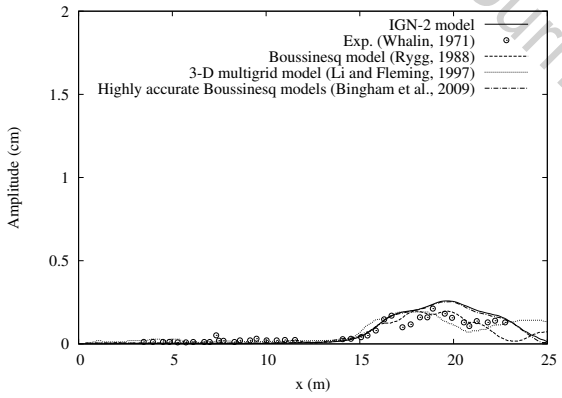

(c) 3rd harmonic

Figure 9: Wave amplitudes along the centerline of the wave tank for Case 3.

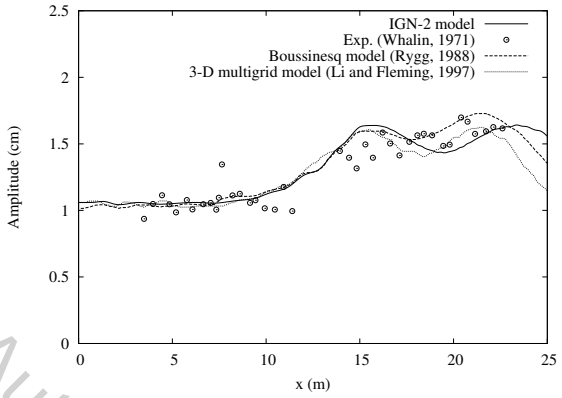

(a) 1st harmonic

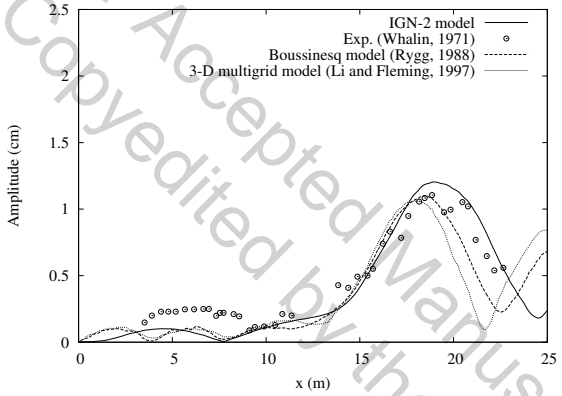

(b) 2nd harmonic

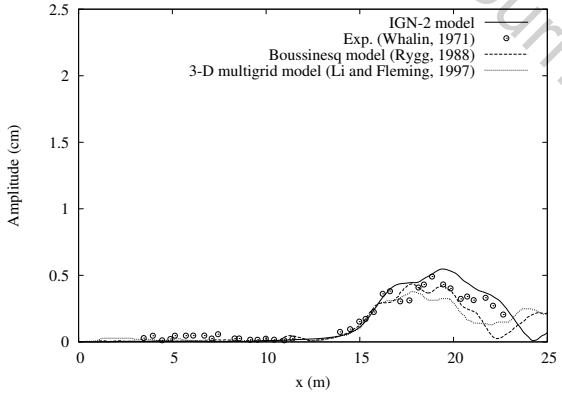

(c) 3rd harmonic

Figure 10: Wave amplitudes along the centerline of the wave tank for Case 4.

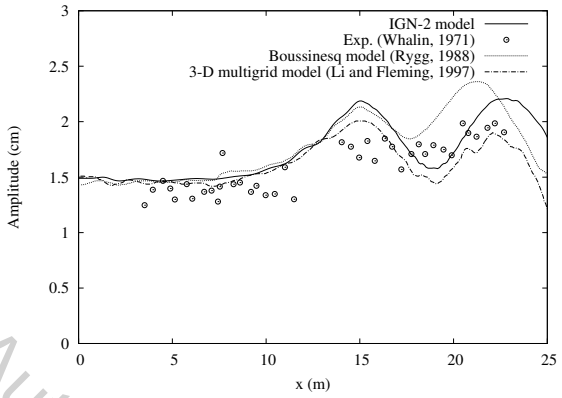

(a) 1st harmonic

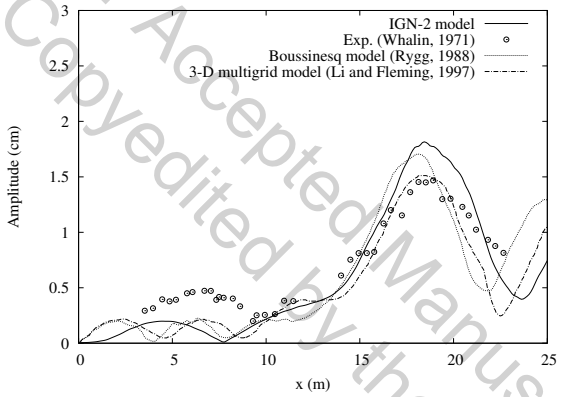

(b) 2nd harmonic

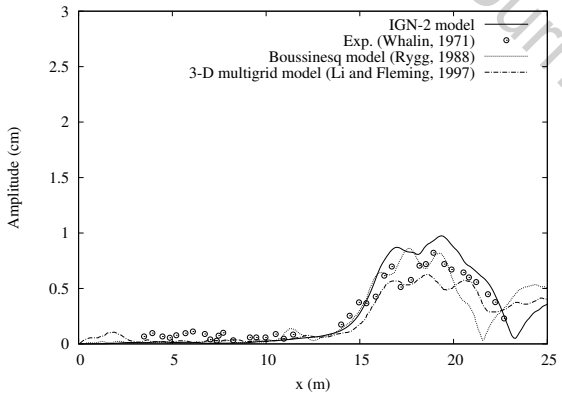

(c) 3rd harmonic

Figure 11: Wave amplitudes along the centerline of the wave tank for Case 5.

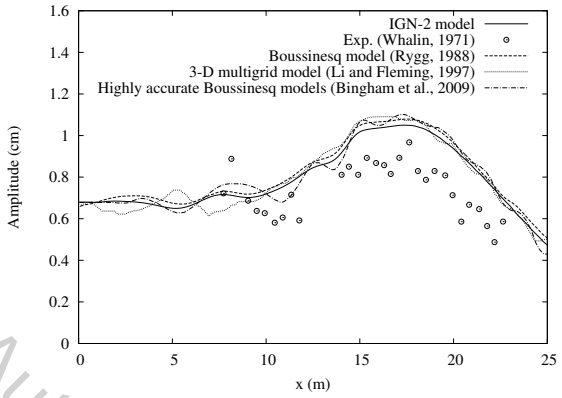

(a) 1st harmonic

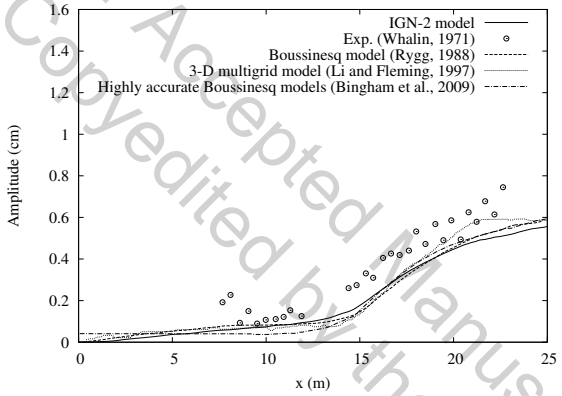

(b) 2nd harmonic

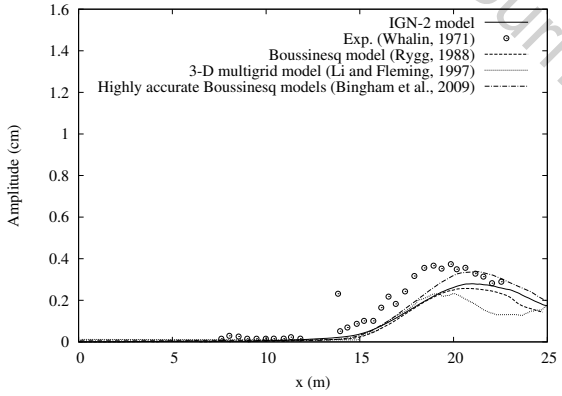

(c) 3rd harmonic

Figure 12: Wave amplitudes along the centerline of the wave tank for Case 6.

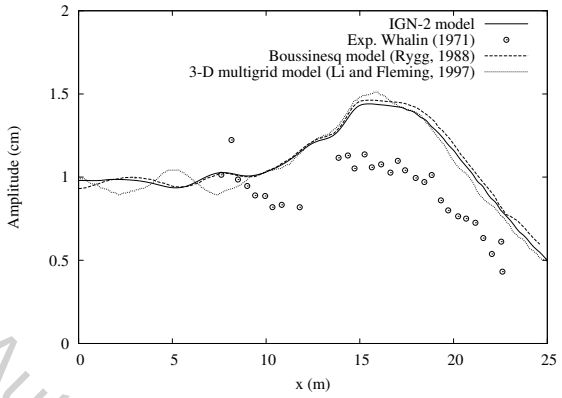

(a) 1st harmonic

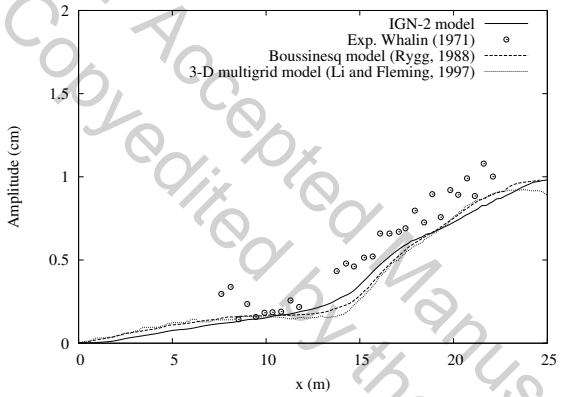

(b) 2nd harmonic

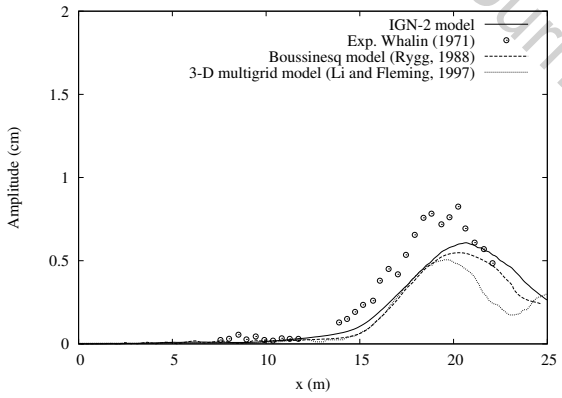

(c) 3rd harmonic

Figure 13: Wave amplitudes along the centerline of the wave tank for Case 7.

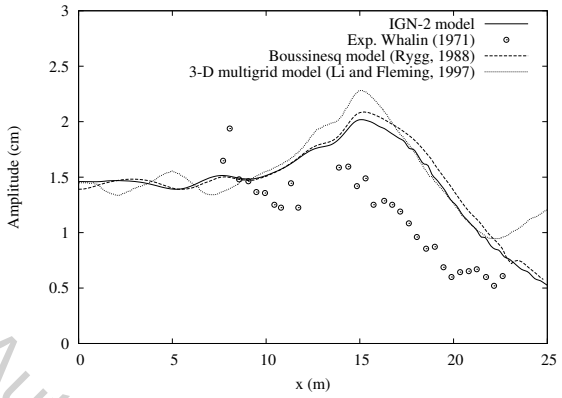

(a) 1st harmonic

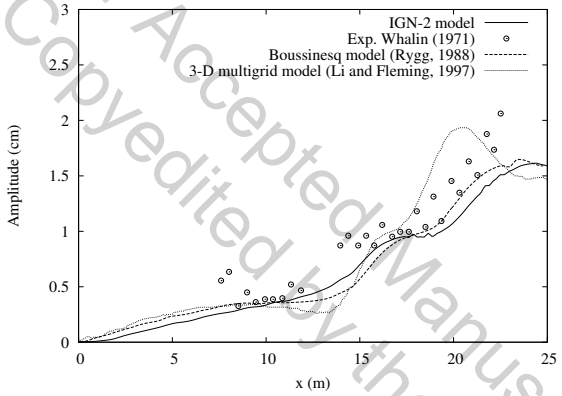

(b) 2nd harmonic

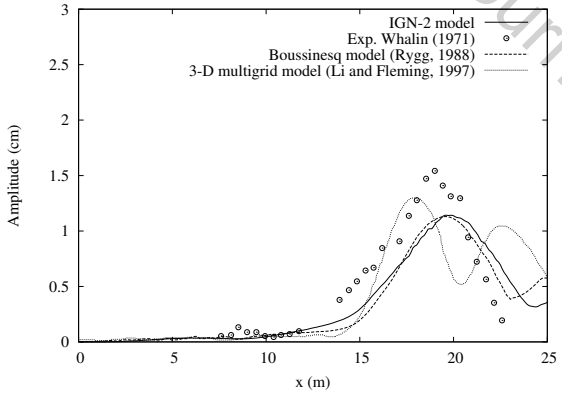

(c) 3rd harmonic

Figure 14: Wave amplitudes along the centerline of the wave tank for Case 8.

6. Conclusions

A numerical model to solve the three-dimensional IGN-2 equations are introduced and applied to some wave diffraction and refraction problems. The solution of the IGN-2 equations are also provided. Here, we present three test cases to study the accuracy of the IGN-2 equations. The first case is on wave evolution in a closed basin. The IGN-2 results show good agreement with the linear analytical solution for small wave heights. In the second test case, we numerically recreated the experiments of Chawla and Kirby (1996) on wave diffraction due to a three-dimensional circular shoal. A close agreement between the IGN-2 equations, the laboratory data (Chawla and Kirby, 1996) and the Boussinesq equations (Chen et al., 2000) is observed.

In the last test case, we reproduce the experiments of Whalin (1971) numerically. Whalin (1971) conducted three sets of experiments by generating waves with periods of $1s$, $2s$ and $3s$, and also with different amplitudes, see Table 1. In all these cases, the fully nonlinear multigrid model (Li and Fleming, 1997) does not produce accurate results but the IGN-2 results agree well with the highly accurate Boussinesq results (Bingham et al., 2009) and the experimental data. It is shown that the IGN-2 results are very accurate for different wave lengths and wave amplitudes. For cases when $T = 2s$, the Boussinesq equations (Rygg, 1988) underpredict the results compared with the IGN-2 results and the highly accurate Boussinesq results (Bingham et al., 2009). Only for cases with $T = 3s$, the Boussinesq equations (Rygg, 1988) provide close results with the IGN-2. This is not surprising because the Boussinesq equations of Rygg (1988) assume weak dispersion. The strongly nonlinear IGN-2 equations give errors of less than 2% in phase velocity from shallow-water depths up to $kd = 4.87$. The IGN-2 equations do not have a restriction on the wave amplitude; they can simulate waves up to breaking.

It is concluded that for many coastal engineering problems, the IGN-2 equations are more suitable than a number of other perturbation-based methods because of the higher accuracy and simplicity of the theory.

Acknowledgement

The work is supported by the National Natural Science Foundation of China (Nos. 11572093, 11772099, 51490671), International Science and Technology Cooperation Project sponsored by National Ministry of Science and Technology of China (No. 2012DFA70420), the Special Fund for Basic Scientific Research of Central Colleges (Harbin Engineering University), the Heilongjiang Touyan Innovation team Program.

References

References

Bingham, H.B., Madsen, P.A., Fuhrman, D.R., 2009. Velocity potential formulations of highly accurate Boussinesq-type models. Coastal Engineering 56, 467–478.

Chawla, A., Kirby, J.T., 1996. Wave transformation over a submerged shoal. Technical Report. CACR Rep. No. 96-03, Dept. of Civ. Engrg., University of Delaware, Newark, Del.

Chen, Q., Kirby, J.T., Dalrymple, R.A., Kennedy, A.B., Chawla, A., 2000. Boussinesq modeling of wave transformation, breaking, and runup. II: 2D. J. of Waterway, Port, Coastal, and Ocean Engineering 126, 48–56.

Demirbilek, Z., Webster, W.C., 1992. Application of the Green-Naghdi theory of fluid sheets to shallow-water waves, Report 1, Model formulation. US Army Wat. Exp. Sta., Coastal Engng. Res. Cntr., Vicksburg, Technical Report No. CERC-92-11 .

Engsig-Karup, A.P., Hesthaven, J.S., Bingham, H.B., Warburton, T., 2008. DG-FEM solution for nonlinear wave-structure interaction using Boussinesq-type equations. Coastal Engineering 55, 197–208.

Ertekin, R.C., Hayatdavoodi, M., Kim, J.W., 2014. On some solitary and cnoidal wave diffraction solutions of the Green–Naghdi equations. Applied Ocean Research 47, 125–137.

Ertekin, R.C., Sundararaghavan, H., 2003. Refraction and diffraction of nonlinear waves in coastal waters by the Level I Green-Naghdi equations, in: Proc. 22nd Int. Conf. on Offshore Mechanics and Arctic Engineering (OMAE 2003), June 8-13, Cancun, Mexico.

Ertekin, R.C., Webster, W.C., Wehausen, J.V., 1986. Waves caused by a moving disturbance in a shallow channel of finite width. J. Fluid Mechanics 169, 275–92.

Eskilsson, C., Sherwin, S.J., 2006. Spectral/hp discontinuous Galerkin methods for modelling 2D Boussinesq equations. J. of Computational Physics 212, 566–589.

Green, A.E., Laws, N., Naghdi, P.M., 1974. On the theory of water waves. Proc. Roy. Soc. of London. A. Mathematical and Physical Sciences 338, 43–55.

Green, A.E., Naghdi, P.M., 1976. Directed fluid sheets. Proc. Roy. Soc. of London. A. Mathematical and Physical Sciences 347, 447–473.

Hayatdavoodi, M., Neill, D.R., Ertekin, R.C., 2018. Diffraction of cnoidal waves by vertical cylinders in shallow water. Theoretical and Computational Fluid Dynamics 32,8, 561–591.

Kennedy, A.B., Fenton, J.D., 1996. A fully nonlinear 3D method for the computation of wave propagation. Coastal Engineering Proceedings 1, 1102–1115.

Kim, J.W., Bai, K.J., Ertekin, R.C., Webster, W.C., 2001. A derivation of the Green-Naghdi equations for irrotational flows. J. Engineering Mathematics 40, 17–42.

Kim, J.W., Bai, K.J., Ertekin, R.C., Webster, W.C., 2003. A strongly-nonlinear model for water waves in water of variable depth—the Irrotational Green-Naghdi model. J. Offshore Mechanics and Arctic Engineering 125, 25–32.

Kim, J.W., Ertekin, R.C., Bai, K.J., 2010. Linear and nonlinear wave models based on Hamilton's principle and stream-function theory: CMSE and IGN. J. Offshore Mechanics and Arctic Engineering 132, 021102.

Li, B., Fleming, C.A., 1997. A three dimensional multigrid model for fully nonlinear water waves. Coastal Engineering 30, 235–258.

Neill, D.R., Ertekin, R.C., 1997. Diffraction of solitary waves by a vertical cylinder: Green-Naghdi and Boussinesq equations, in: Proc. 16th Int. Conf. on Offshore Mechanics and Arctic Engineering, OMAE '97, January, Yokohama, Japan, pp. 63–71.

Neill, D.R., Hayatdavoodi, M., Ertekin, R.C., 2018. On solitary wave diffraction by multiple, in-line vertical cylinders. Nolinear Dynamics 91,2, 975–994.

Rygg, O.B., 1988. Nonlinear refraction-diffraction of surface waves in intermediate and shallow water. Coastal Engineering 12, 191–211.

Wei, G., Kirby, J.T., 1995. Time-dependent numerical code for extended Boussinesq equations. J. Waterway, Port, Coastal, and Ocean Engineering 121, 251–261.

Whalin, R., 1971. The limit of applicability of linear wave refraction theory in a convergence zone. Res. Rep. H-71-3. U. S. Army Corps of Engrs. Waterways Expt. Station, Vicksburg .

Wiegel, R.L., 1964. Oceanographical Engineering. Prentice-Hall International Englewood Cliffs, NJ.

Young, C.C., Wu, C.H., Liu, W.C., Kuo, J.T., 2009. A higher-order non-hydrostatic σ model for simulating non-linear refraction–diffraction of water waves. Coastal Engineering 56, 919–930.

Zhao, B.B., Duan, W.Y., Ertekin, R.C., 2014. Application of higher-level GN theory to some wave transformation problems. Coastal Engineering 83, 177–189.

Zhao, B.B., Duan, W.Y., Ertekin, R.C., Hayatdavoodi, M., 2015a. High-level Green–Naghdi wave models for nonlinear wave transformation in three dimensions. J. of Ocean Engineering and Marine Energy 1, 121–132.

Zhao, B.B., Ertekin, R.C., Duan, W.Y., 2015b. A comparative study of diffraction of shallow-water waves by high-level IGN and GN equations. J. of Computational Physics 283, 129–147.

Zhao, B.B., Duan, W.Y., Demirbilek, Z., Ertekin, R.C.,Webster, W.C., 2016. A comparative study between the IGN-2 equations and the fully nonlinear, weakly dispersive Boussinesq equations. Coastal Engineering, 111, 60–69.